ACS APPLIED MATERIALS & INTERFACES

www.acsami.org

Research Article

KAT Ligation for Rapid and Facile Covalent Attachment of Biomolecules to Surfaces

Alessandro Fracassi, Ankita Ray, Nako Nakatsuka, Cristiana Passiu, Matthias Tanriver, Dominik Schauenburg, Simon Scherrer, Anissa Ould Chaib, Joydeb Mandal, Shivaprakash N. Ramakrishna, Jeffrey W. Bode, Nicholas D. Spencer, Antonella Rossi, and Yoko Yamakoshi*

Cite This: *ACS Appl. Mater. Interfaces* 2021, 13, 29113–29121

Read Online

ACCESS | Metrics & More | Article Recommendations | Supporting Information

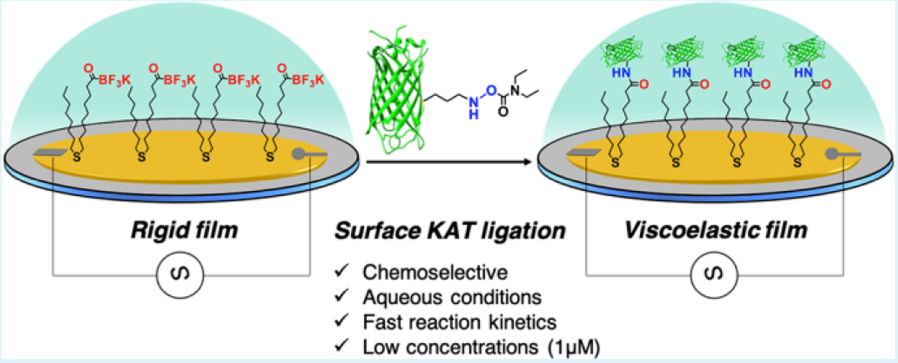

ABSTRACT: The efficient and bioorthogonal chemical ligation reaction between potassium acyltrifluoroborates (KATs) and hydroxylamines (HAs) was used for the surface functionalization of a self-assembled monolayer (SAM) with biomolecules. An alkane thioether molecule with one terminal KAT group (**S-KAT**) was synthesized and adsorbed onto a gold surface, placing a KAT group on the top of the monolayer (**KAT-SAM**). As an initial test case, an aqueous solution of a hydroxylamine (HA) derivative of poly(ethylene glycol) (PEG) (**HA-PEG**) was added to this **KAT-SAM** at room temperature to perform the surface KAT ligation. Quartz crystal microbalance with dissipation (QCM-D) monitoring confirmed the rapid attachment of the PEG moiety onto the SAM. By surface characterization methods such as contact angle and ellipsometry, the attachment of PEG layer was confirmed, and covalent amide-bond formation was established by X-ray photoelectron spectroscopy (XPS). In a proof-of-concept study, the applicability of this surface KAT ligation for the attachment of biomolecules to surfaces was tested using a model protein, green fluorescent protein (GFP). A GFP was chemically modified with an HA linker to synthesize **HA-GFP** and added to the **KAT-SAM** under aqueous dilute conditions. A rapid attachment of the GFP on the surface was observed in real time by QCM-D. Despite the fact that such biomolecules have a variety of unprotected functional groups within their structures, the surface KAT ligation proceeded rapidly in a chemoselective manner. Our results demonstrate the versatility of the KAT ligation for the covalent attachment of a variety of water-soluble molecules onto SAM surfaces under dilute and biocompatible conditions to form stable, natural amide bonds.

KEYWORDS: *potassium acyltrifluoroborate (KAT) ligation, self-assembled monolayer, bioorthogonal surface reaction, bioactive surfaces, monitoring real-time assembly*

1. INTRODUCTION

The immobilization of biomolecules onto surfaces in well-organized, reproducible ways is critical for the design of biosensors.[1] Site-specific attachment ensures optimal orientation of biomolecules (e.g., protein- or DNA-based recognition elements) on the surface and allows the active binding site to be exposed to the analyte with reduced steric hindrance, resulting in higher sensitivity for biomarker diagnostics.[2] To immobilize biomolecules onto surfaces in a highly ordered manner, self-assembled monolayer (SAM) techniques are often used.[3] These SAMs are assembled onto surfaces with a defined orientation of the biomolecules by selective bond formation

Received: March 26, 2021
Accepted: May 31, 2021
Published: June 9, 2021

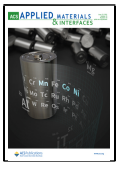

https://doi.org/10.1021/acsami.1c05652
ACS Appl. Mater. Interfaces 2021, 13, 29113–29121

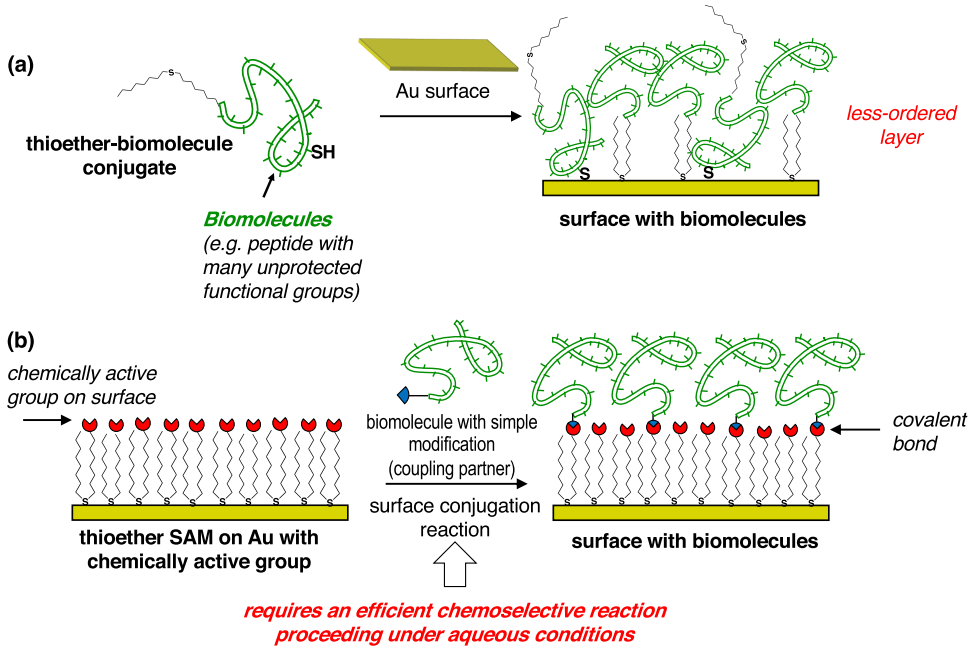

Figure 1. Strategies for the formation of self-assembled monolayers (SAMs) with biomolecules. (a) Synthesis of the conjugates of Au-reactive alkyl thioethers and biomolecules, followed by the reaction with a Au surface. (b) Initial formation of a SAM with chemically reactive groups on Au and subsequent coupling with biomolecules. The layers of biomolecules formed using the strategy (b) are expected to be better ordered than by (a) with a controlled orientation.

between the flat metal surface (e.g., Au or Ag) with functional groups (e.g., thiol, thioether, or disulfide).

Conventional methods to form SAMs with biomolecules involve one of the two strategies:[4] (1) syntheses of biomolecule−alkyl anchor conjugates incorporating a group that reacts with the metal (such as the sulfur-containing groups mentioned above) and attachment onto the metal surface to form a SAM (Figure 1a) and (2) initial formation of SAMs on the metal surfaces with active functionalities available for subsequent reactions to attach the biomolecules (Figure 1b). In the first case, there is some risk that the biomolecule itself (e.g., cysteine-containing peptides) may react with Au, thereby disturbing the selective reaction of sulfur groups with the metal surface, which is essential to achieve a uniform orientation of the surface-attached biomolecules (Figure 1a). In the second case, once the functionalizable scaffold SAM has been preformed on a metal surface in a suitable orientation, exposing the active groups to the solvent, with the help of selective sulfur-metal reactions and van der Waals interaction of alkyl chains, diverse, minimally modified biomolecules can be coupled to form a wide variety of biofunctionalized surfaces (Figure 1b). The latter method can be ideal to facilitate the development of biosensing devices that require different chemistries for attaching recognition elements or biomolecules.[2,5] An important criterion for such a SAM scaffold is the presence of chemically active groups that enable stable and robust attachments, ideally via covalent linkage to the biomolecule with fast kinetics and high yield in a chemoselective manner. Further application of this approach would also incorporate the immobilization of a nonfouling background (Figure 1b).[6]

A variety of chemical transformations have been used for the covalent attachment of organic or biological molecules to preform SAMs on surfaces. These reactions include Diels−Alder reaction with benzoquinone,[7] conjugation with phenylisocyanate,[8] reaction of boronic acid and diols,[9] amide-forming reaction from *N*-hydroxysuccinimide (NHS)-activated carboxylic acids, Michael addition, reductive amination, Staudinger-type ligation, Cu(I)-catalyzed azide-alkyne click chemistry,[10] strain-promoted azide-alkyne cycloaddition,[11,12] and radical nitroxide exchange reaction.[13] Among these reactions, we have previously used Cu(I)-catalyzed click chemistry for the chemical functionalization of Au-coated atomic force microscopy (AFM) tips prefunctionalized with a tripod molecule having a terminal alkyne group.[14] However, many of these reactions require coupling reagents, metal catalysts, high temperatures, large amounts of expensive biomolecules, and do not always proceed in high yields, especially under physiological conditions, in which biomolecules can remain intact. Such reactions would enable the facile assembly of biomolecules on the surface in situ by simply adding the reactant to the SAM to develop bioactive surfaces preserving the activities of the biomolecules.

To this end, potassium acyltrifluoroborate (KAT) ligation, a relatively new amide-forming reaction between a molecule with a KAT moiety and hydroxylamine (HA) derivatives, was investigated. When the biomolecule of interest was used for surface functionalization, HA-linker-modified biomolecules can be immobilized via a surface KAT ligation reaction. The KAT ligation has been intensively studied in the solution phase and has proven to be rapid under aqueous conditions, with second-order rate constants up to 22 M^{-1} s^{-1}, especially under acidic conditions.[15] It was used in the ligation reaction of unprotected biomolecules to quantitatively provide modified peptides[16] and proteins[17] as products. Furthermore, the reaction can be performed at low concentrations of the reactants, forming natural amide bonds without involving coupling reagents or producing toxic byproducts. Our recent results also demonstrated this approach successfully provides hybrid nanoparticles for in vivo imaging.[18,19] The use of KAT

https://doi.org/10.1021/acsami.1c05652
ACS Appl. Mater. Interfaces 2021, 13, 29113−29121

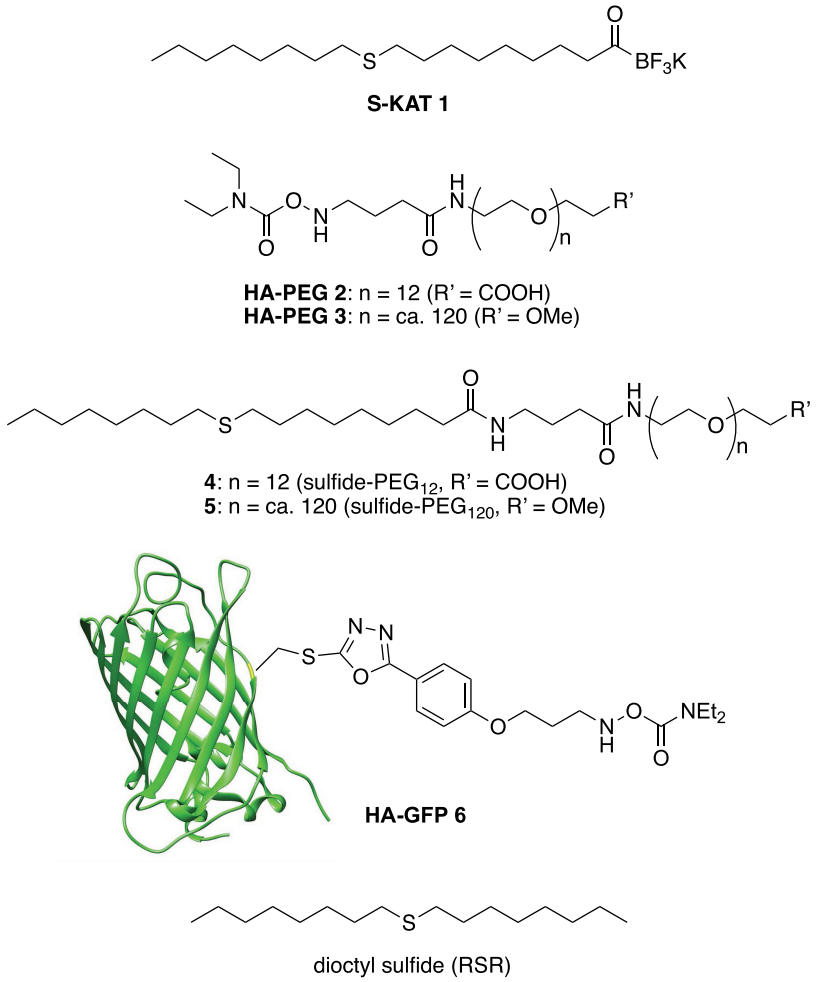

Figure 2. Structures of the molecules used in the formation of self-assembled monolayer (SAM) and chemical modification.

ligation in surface modification was thought to provide several advantages compared to other chemical reactions. The chemoselective and orthogonal KAT ligation reaction could facilitate surface modification with biomolecules bearing unprotected functional groups. In this proof-of-concept study, KAT ligation was used for the covalent functionalization of planar surfaces of self-assembled monolayers (SAM) with unprotected biomolecules, facilitating the development of bioactive surfaces.

2. EXPERIMENTAL SECTION

2.1. Synthesis of S-KAT 1. A thioether molecule with a terminal KAT group (**S-KAT 1** in Figure 2) was synthesized from dibromooctane as a starting material (Scheme S1). The obtained compound **1** was purified, and characterized by HR-MS, IR, and ^{1}H, ^{13}C, ^{19}F, and ^{11}B NMR.

2.2. Synthesis of HA Derivatives of PEG (HA-PEG 2 and 3). The *N*-Boc-protected precursor of **HA-PEG 2** (Figure 2) was synthesized as shown in Scheme S2, purified and characterized by high-resolution mass spectrometry (HR-MS), IR, and ^{1}H ^{13}C NMR. The final deprotection process was carried out with trifluoroacetate (TFA) and monitored by liquid chromatography−mass spectrometry (LC−MS) (Figure S18). Upon completion of the deprotection, TFA was removed in vacuo from the reaction mixture and the product was used without further purification. **HA-PEG 3** was prepared in a similar manner (Scheme S3).

2.3. Synthesis of Sulfide-PEG12 (4) and Sulfide-PEG120 (5). As the control compounds for ellipsometry measurements, sulfide-PEG12 **4** and sulfide-PEG120 **5** (Figure 2) were synthesized in solution phase (Schemes S4 and S5).

2.4. Synthesis of HA Derivative of GFP 6. HA-GFP 6 (Figure 2) was prepared according to the reported method with slight modifications (Scheme S6).[17] Briefly, a mutant (S147C) of superfolder green fluorescent protein (sfGFP), bearing a single accessible thiol, was expressed in an *Escherichia coli* host BL21 (DE3) and purified by sequential Ni-affinity and anion-exchange chromatography. The methylsulfonephenyl-oxadiazole linker (**S10** in scheme S6), which has been reported to react chemoselectively with cysteine side chains in proteins, was synthesized according to the reported method[17] and subjected to a reaction with the cysteine side chain of sfGFP-S147C to obtain **HA-GFP 6**. The prepared **HA-GFP 6** was immediately used for the surface KAT ligation reaction of **KAT-SAM**.

2.5. Preparation of KAT-SAM on Gold. The 50 nm gold substrates were prepared by vapor deposition of gold on microscopic glass slides, which were precoated with a 10 nm chromium layer. The gold substrate was soaked in a solution of **S-KAT 1** (1 mM in EtOH) for 20 h at room temperature. The surface was thoroughly washed with EtOH.

2.6. Surface KAT Ligation of KAT-SAM with HA-PEG 2 or 3. KAT-SAM on gold was soaked in a solution of **HA-PEG 2** or **3** (0.5 mM in pH 5.5 phosphate buffer (PB)) for 30 min or 16 h at room temperature. The surface was thoroughly washed with Milli-Q water and EtOH and subjected to contact angle, ellipsometry, and XPS analyses.

2.7. Contact Angle Measurement. Static water contact angles were measured by a goniometer (Ramé Hart, Inc.) at three different spots on each sample. Samples were prepared by on-surface KAT ligation on **KAT-SAM** with **HA-PEG 2** or **3**. As a control experiment,

https://doi.org/10.1021/acsami.1c05652
ACS Appl. Mater. Interfaces 2021, 13, 29113−29121

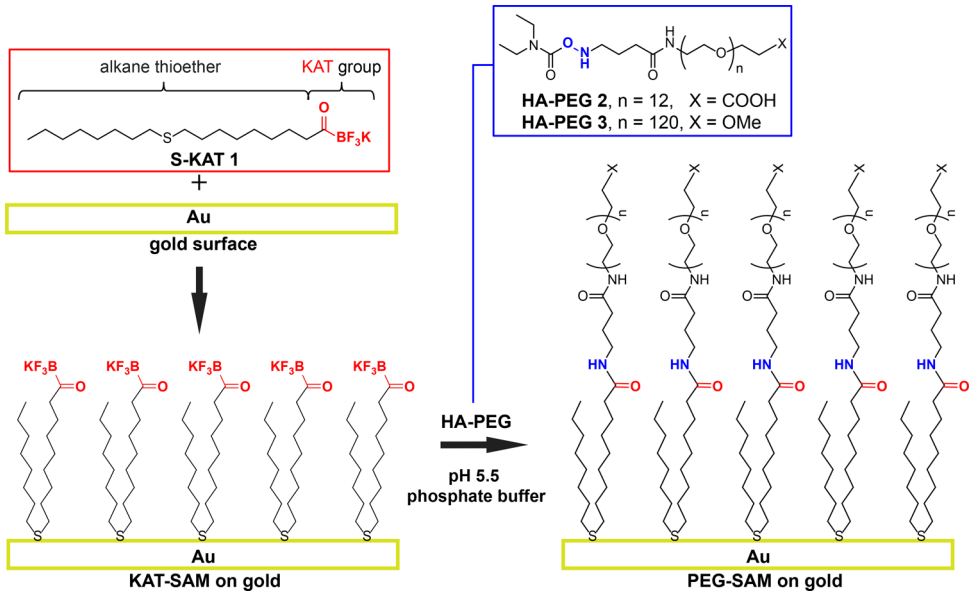

Figure 3. Schematic illustration of initial SAM formation with thioether **1** (**S-KAT**) on Au surface (**KAT-SAM**) and subsequent in situ KAT ligation with HA-poly(ethylene glycol) (PEG) derivatives **2** and **3**.

a SAM with dioctyl sulfide was prepared on gold and subjected to the reaction with **HA-PEG 2**.

2.8. Ellipsometry. Ellipsometric data were obtained on a VASE M-2000F spectroscopic ellipsometer (LOT Oriel GmbH). Five measurements were performed on each sample. The average distance between chains (L) was estimated according to a previous report[20] using the following equation

$$L = ((M/\rho_{dry} dN_A))^{1/2} \quad (1)$$

where M is the PEG molecular weight, ρ_{dry} is the density of the dry PEG layer, d is the average layer thickness determined by ellipsometry, and N_A is Avogadro's number. The grafting density (nPEG), defined as (chains/nm^2), was estimated assuming a hexagonal (close-packed) pattern from the equation

$$n\text{PEG} = 2/(\sqrt{3}L^2) \quad (2)$$

The dimension of the attached biomolecules was estimated calculating the radius of gyration (R_g) by the empirical equation below

$$R_g = 0.181\, N^{0.58}(\text{nm}) \quad (3)$$

where N is the number of ethylene glycol repeat units.

2.9. X-ray Photoelectron Spectroscopy (XPS). A PHI Quantera SXM spectrometer (ULVAC-PHI, Chanhassen, MN) was used for the XPS measurements. The information about the spectrometer and the settings applied for acquiring the spectra are provided in the SI.

2.10. Quartz Crystal Microbalance with Dissipation (QCM-D). The QCM-D measurements were carried out using a Q-sense analyzer (Biolin Scientific AB) with a gold-coated quartz crystal cleaned by UV/ozone treatment. After initially stabilizing the sensor in EtOH (step 1 in Figure 5), an EtOH solution of **S-KAT 1** (1 mM) was injected (step 2) into the cell. After the frequency change plateaued, the surface was washed by EtOH injection to remove the unbound **S-KAT 1** (step 3). The solvent in the cell was replaced with water (step 4) and then with phosphate buffer (pH 5.5) (step 5). Subsequently, a solution of **HA-PEG 3** (0.1 mM in pH 5.5 phosphate buffer) was injected into the cell (step 6). The frequency decrease was observed to correspond to the on-surface KAT ligation reaction. Finally, phosphate buffer (pH 5.5) was injected into the cell to remove unbound **HA-PEG 3** from the surface (step 7). The surface reaction with **HA-GFP 6** was carried out in a similar manner with 1 μM of **6** in pH 4.0 citrate buffer (Figure 8).

3. RESULTS AND DISCUSSION

As a compound for the formation of a chemically active SAM scaffold, a dialkyl thioether derivative with one terminal KAT group (**S-KAT 1** in Figure 2) was synthesized. We initially prepared a SAM of **1** (**KAT-SAM**) on the gold surface and subsequently performed the on-surface KAT ligation with HA derivatives of biomolecules. As a model system, HA derivatives of a water-soluble polymer, poly(ethylene glycol) (PEG) (**HA-PEG 2** and **3** in Figure 2), were subjected to the surface ligation reaction. The reaction process was monitored in real time by QCM-D, and the resulting surfaces (**PEG-SAM**) were carefully characterized by contact angle measurements, ellipsometry, and XPS. Finally, the *on-surface* KAT ligation was performed using a biomolecule—an HA derivative of green fluorescent protein (GFP, **HA-GFP 6** in Figure 2)—to demonstrate the suitability of this ligation reaction for the in situ attachment of biomolecules (Figure 3).

3.1. Contact Angle Measurements. Static water contact angles were measured on a **KAT-SAM** surface and a **PEG-SAM** surface prepared by the addition of **HA-PEG 2** or **3** in pH 5.5 phosphate buffer. As a control experiment, a SAM with dioctyl sulfide (**RSR SAM**) was prepared on a gold substrate and treated in a solution of **HA-PEG 2** in the same buffer. As shown in Figure 4a, while the contact angle of the negative control **RSR SAM** surface—without the KAT moiety—showed a relatively higher value (87°), the **KAT-SAM** surface with adsorbed **S-KAT 1** showed a contact angle of 55°. These findings are in line with our expectation, showing that the presence of KAT renders the surface more hydrophilic. After the addition of **HA-PEG 2** or **3** to the **KAT-SAM**, the contact angle further decreased to lower values (44 and 46°, respectively), indicating the stable attachment of hydrophilic PEG moieties to the surface. On the other hand, the **RSR SAM** retained a hydrophobic contact angle value (86°) after addition of **HA-PEG 2**, suggesting that there was no stable attachment of PEG moieties to the surface. Taken together, the

https://doi.org/10.1021/acsami.1c05652
ACS Appl. Mater. Interfaces 2021, 13, 29113−29121

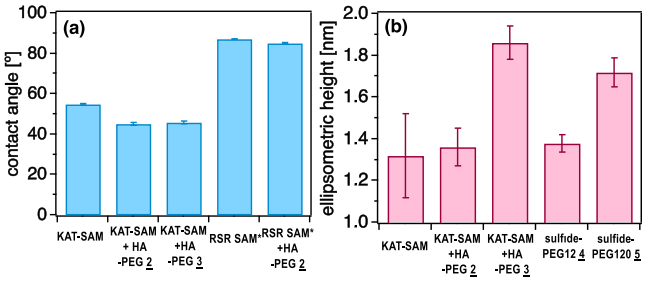

Figure 4. (a) Contact angle data of **KAT-SAM** and control SAM (**RSR** (dioctyl sulfide) **SAM**) before and after the addition of **HA-PEG 2** or **3**. (b) Ellipsometry data of **KAT-SAM** and after the addition of **HA-PEG 2** or **3** and control SAM prepared with ligation products sulfide-PEG12 **4** or sulfide120 **5** (synthesized in solution phase from **S-KAT 1** and **HA-PEG 2** or **3**, respectively).

decreased contact angle values in the **KAT-SAM** after the addition of **HA-PEG** verified the stable attachment of PEG, presumably via covalent bonds.

3.2. Ellipsometry. Ellipsometry was used to estimate the thickness of monolayers before and after the addition of **HA-PEG** to the **KAT-SAM**. As shown in Figure 4b, ellipsometry data corroborated the contact angle data. The estimated thickness of the **KAT-SAM** surfaces (1.30 nm) increased after the addition of **HA-PEG 2** (1.35 nm) or **HA-PEG 3** (1.86 nm). Importantly, these values were in good agreement with the values of control SAMs that had been prepared by exposing a gold surface to the ligation products, sulfide-PEG12 **4** and sulfide-PEG120 **5**, which were already synthesized in the solution phase (Figure 4b). The relatively small increase in the thickness of the SAM following ligation with **HA-PEG 2**—which has shorter PEGs—was likely due to the tangling of the PEG moiety on the SAM during the drying process of the samples prior to ellipsometry measurements. Using longer PEG (PEG120), the increase of the monolayer thickness upon addition of HA-PEG was observed to be more significant and in good agreement with the thickness of a monolayer prepared from ligation product **5** (1.71 nm).[21] The extent of packing on the surface was evaluated by considering the ratio between the spacing (L) separating two attached PEG chains and twice the radius of gyration (R_g).[20,22] In densely packed layers (brush regime), where the overlapping of R_g of neighboring chains occurs, the spacing between two attached chains is lower than $2R_g$ ($L < 2R_g$), providing values of $L/2R_g < 1$. Conversely, in nondensely packed layers (mushroom-like regime), where the R_g of neighboring chains do not overlap, the spacing between two attached chains is higher than $2R_g$ ($L > 2R_g$), providing values of $L/2R_g > 1$. Based on the average thickness values determined by ellipsometry, the PEG layer obtained after functionalization of KAT-SAM with **HA-PEG 3** was around 0.07 chains/nm^2, which corresponds to a spacing, L between chains of 3.8 nm. The value of R_g for a 5 kDa PEG chain was calculated to be 2.9 nm, determining an $L/2R_g$ of about 0.7. This result suggests that the PEG layer obtained is in the brush regime.

3.3. QCM-D Monitoring. To monitor the reaction of **KAT-SAM** surfaces with **HA-PEG** in real time, QCM-D measurements were performed. QCM-D is a mass-sensitive technique that uses the piezoelectric properties of a quartz crystal that oscillates upon application of a voltage.[23] When biomolecules are assembled onto the sensor surface, the oscillating mass increases, which results in a decrease in the resonance frequency of the crystal oscillations.[24] Further, the variation in energy dissipation is simultaneously measured, which provides information on the viscoelastic properties of the assembled layer at the sensor surface. To see clear changes in the resonance, **HA-PEG 3** with a relatively large PEG moiety was investigated (Figures 5 and S28).

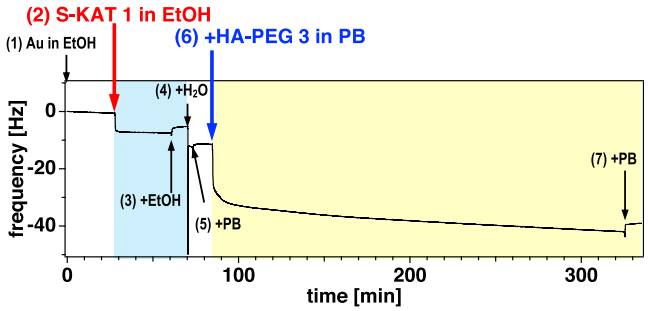

Figure 5. QCM-D traces upon formation of SAM with **S-KAT 1** and subsequent KAT ligation with **HA-PEG 3** in phosphate buffer (PB). (1) The crystal oscillation frequency was recorded in EtOH. (2) Changes in the frequency were monitored upon injection of **S-KAT 1** (1 mM in EtOH). (3) EtOH rinse step. (4) Exchange with water. (5) Exchange with pH 5.5 PB. (6) Addition of **HA-PEG 3** (0.1 mM) in pH 5.5 PB. (7) Final rinse with PB. The layer thickness of each assembled layer was approximated by the simulation shown in the SI (Figure S28).

The thickness of the **KAT-SAM** surface initially formed on the gold surface was evaluated based on the frequency change observed during the process in step (2) in Figure 5. When the layer of the molecules deposited on the QCM-D sensor is rigid and a laterally homogeneous film, it is possible to neglect the dissipated energy.[25] Thus, the observed frequency changes can be directly correlated to the mass of the attached material through the Sauerbrey equation.[26] The evaluated initial **SAM-KAT** formation on gold provided the thickness of the layer to be ca. 2.2 nm.[27] On the other hand, after the addition of **HA-PEG 3** (step 6 above), a nonrigid, viscoelastic film was formed, as observed by the significant increase in dissipation energy (Figure S28a), indicating the formation of a flexible coating. In such a case, where the Sauerbrey equation no longer holds, the use of a viscoelastic model (Voigt model)[25,28] for thickness estimation was required (Figure S28b,c). The thickness of the **PEG-SAM** monolayers formed after the ligation reaction with **HA-PEG 3** was determined to be 3.5 nm.

3.4. XPS Analyses. To confirm the amide formation by KAT ligation of the **KAT-SAM** with HA derivatives, XPS measurements were employed on the surfaces before and after the addition of the HA derivatives. For this experiment, **HA-PEG 2** with a shorter PEG, which was expected to show less intense peaks corresponding to PEG O−C−O moieties, and will therefore not obscure other peaks, was used to detect the amide formation more clearly. The surfaces of **KAT-SAM**, before and after the addition of **HA-PEG 2**, were probed by XPS.

From the Gaussian−Lorentzian fit of the peaks observed in the XPS spectra (Figures 6 and S25−S27), the relative peak intensities corresponding to each element were estimated, as summarized in Table 1. Upon incubation of the **KAT-SAM** surface for 30 min and 16 h in the presence of **HA-PEG 2**, a visible decrease of F 1s peaks (from 13 to 0%) and K 2p peaks (9.4 to 0%) and a simultaneous increase of N 1s peaks (from

https://doi.org/10.1021/acsami.1c05652
ACS Appl. Mater. Interfaces 2021, 13, 29113−29121

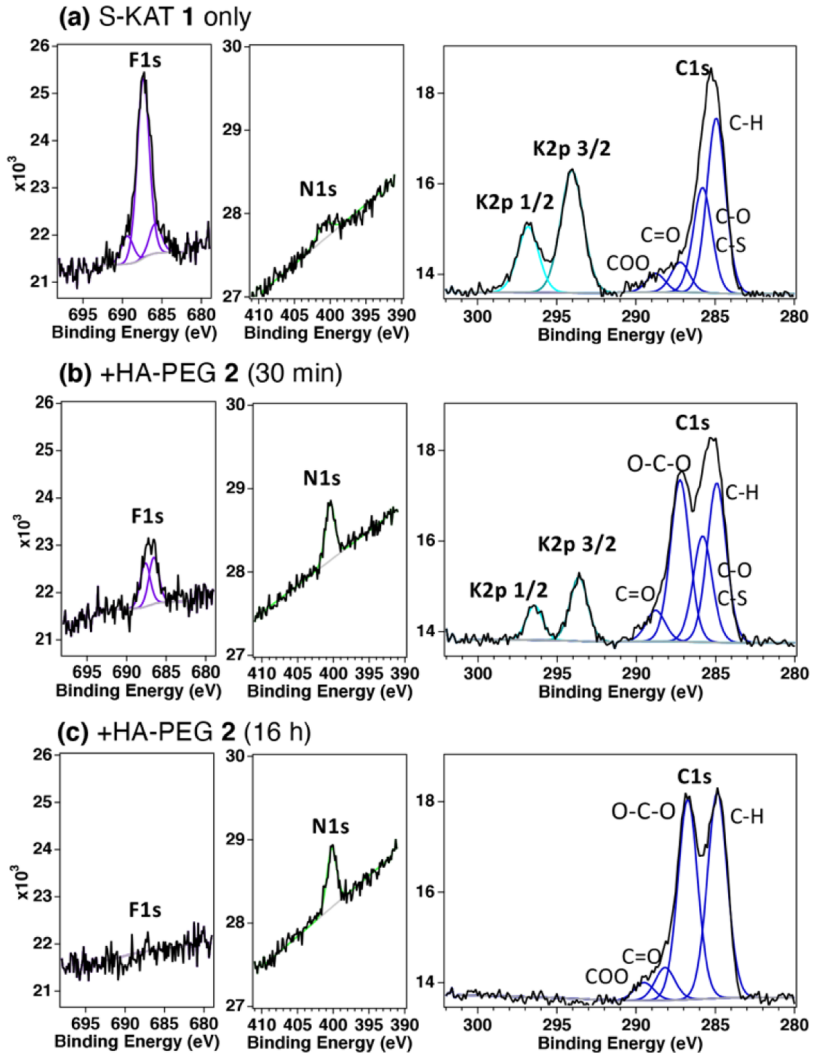

Figure 6. XPS spectra in F 1s, N 1s, K $2p_{1/2}$, K $2p_{3/2}$, and C 1s regions of the SAM surface of S-KAT **1** (a) and after addition of HA-PEG **2** for 30 min (b) and 16 h (c).

Table 1. Relative Peak Intensities from XPS Analysis of Surface with S-KAT 1 on Au, before and after the addition of HA-PEG 2, and RSR on Au, before and after the addition of HA-PEG 2

		elements [%]						
surface		C	O	N	S	F	K	thickness [nm]
1 on Au	experimental	57.6 ± 0.4	13.1 ± 0.5	3.3 ± 0.5	4.5 ± 0.4	12 ± 1[a]	10.0 ± 0.2	1.2 ± 0.1
	theoretical	70.8	4.17	0	4.17	12.5	4.17	
1 on Au + **2**	experimental (30 min)	69 ± 1	16 ± 1	3.6 ± 0.2	4.4 ± 0.2	3.2 ± 0.7[a]	4.1 ± 0.7	1.4 ± 0.2
	experimental (16 h)	73 ± 1	17 ± 1	4.5 ± 0.3	5.0 ± 0.3	nd[b]	nd[b]	1.4 ± 0.2
	theoretical	72.1	24.6	1.64	1.64	0	0	
RSR[c] on Au	experimental	84 ± 1.0	6.7 ± 0.5	nd[b]	9.3 ± 0.2	nd[b]	nd[b]	0.56 ± 0.05
	theoretical	94.1	0	0	5.88	0	0	
RSR[c] on Au + **2**	experimental (16 h)	85 ± 2	3 ± 2	nd[b]	11 ± 1	nd[b]	nd[b]	0.4 ± 0.2

[a]Observed as two components (Figures S25 and S26). [b]nd: not detected. [c]RSR: dioctyl sulfide. Numbers after ± are standard deviation.

1.7 to 3.8%) were observed, suggesting the elimination of the KAT group and the formation of an amide bond by KAT ligation on the surface. Especially, the clear disappearance of the KAT group confirmed that the **KAT-SAM** was formed on the Au surface in the desired orientation with the KAT group on top, presumably due to relatively polar KAT moiety being exposed to the solvent phase—advantageous for an efficient surface KAT ligation at the interface. Furthermore, an increase in the peak intensities of C 1s (from 58 to 72%) and O 1s (from 13 to 17%) was also clearly observed, consistent with the addition of PEG. In contrast, the surface obtained from the reaction of the negative controls **RSR SAM** and **HA-PEG 2** did not show any significant increase of C and O peaks, confirming that their increase in the **KAT-SAM** reaction corresponded to the PEG group being attached via the ligation reaction.

https://doi.org/10.1021/acsami.1c05652
ACS Appl. Mater. Interfaces 2021, 13, 29113−29121

From surface elemental composition analyses from the normalized XPS peak areas, the amount of carbon present on the gold surface (C 1s/Au 4f ratio) was estimated (Figure 7).

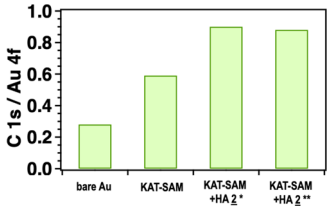

Figure 7. Normalized relative peak intensities of C 1s/Au 4f, observed by XPS spectra of bare gold, **KAT-SAM** surface, and after the addition of **HA-PEG 2** (*30 min and **16 h after).

While the **KAT-SAM** value was 0.59, the results after surface ligation of 30 min and 16 h were 0.90 and 0.88, clearly indicating an increase in carbon corresponding to the addition of PEG molecules on the surface. This result suggests that surface functionalization of **KAT-SAM** was complete within 30 min under the reaction conditions with 0.5 mM of **HA-PEG 2** in pH 5.5 phosphate buffer, in line with previously reported results in solution phase,[15,29] that showed a rapid amide-bond-forming reaction under dilute conditions and with 1:1 stoichiometric ratio of reactants.

3.5. Immobilization of GFP on SAM by Surface KAT Ligation. To investigate the suitability of the surface KAT ligation for the attachment of unprotected biomolecules, we performed surface functionalization of the **KAT-SAM** with green fluorescent protein (GFP) bearing an HA anchor. According to a reported method,[17] a recombinant GFP bearing a surface-exposed cysteine, was chemically functionalized with an HA anchor **S10** to provide **HA-GFP 6** (Scheme S6). The surface ligation reaction with **KAT-SAM** was carried out in pH 4.0 citrate buffer in the presence of 1 μM **HA-GFP 6**.

The entire sequence of the surface reaction, from the initial formation of **KAT-SAM** to the on-surface ligation reaction with the **HA-GFP 6**, was monitored by QCM-D as shown in Figures 8a and S29a. To the surface assembled with **KAT-SAM**, which was subsequently washed with EtOH and exchanged with water and then citrate buffer, 1 μM **HA-GFP 6** in citrate buffer (pH 4.0) was added. An abrupt decrease in the frequency of 25.5 Hz was clearly observed upon addition of **HA-GFP 6**. Quantitative analysis through viscoelastic modeling correlated the variation in frequency and dissipation to an increase in thickness of ca. 4 nm (Figure S29). This value is in line with the reported size of GFP with a length of 4.2 nm and a diameter of 2.2 nm, with a cylindrical shape.[30] As a negative control experiment, dioctyl sulfide SAMs without KAT moieties were prepared and subjected to the addition of **6** while being monitored by QCM-D (Figure 8b). Upon addition of **HA-GFP 6**, a minimal decrease in frequency was observed, which was recovered by washing with citrate buffer, indicating negligible molecular attachment to the surface.

4. CONCLUSIONS

In conclusion, we have demonstrated surface KAT ligation to be a rapid and efficient method for the chemical functionalization of SAMs with biomolecules under physiological conditions. The approach is suitable for the immobilization of small molecules, polymers, and biomolecules such as peptides and proteins with exposed, unprotected functional groups. The method developed in this work should find applications in the modification of surfaces with proteins and for the study of their structure retention, activity, and functionality once conjugated onto surfaces.

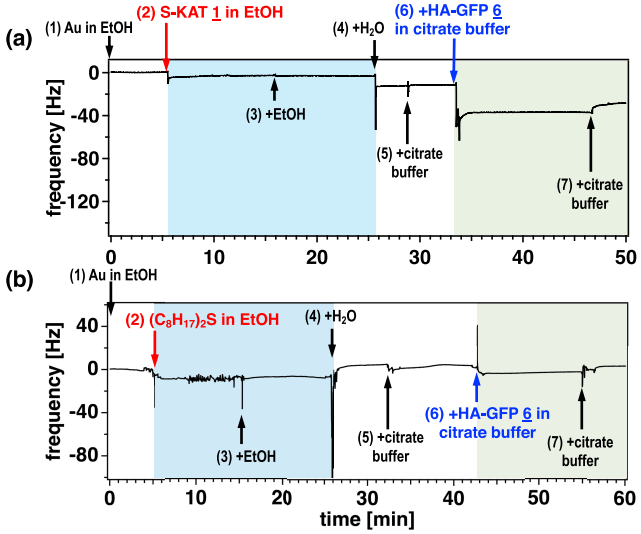

Figure 8. (a) Quartz crystal microbalance (QCM) traces upon treatment with **S-KAT 1** in EtOH and subsequent KAT ligation with **HA-GFP 6** in citrate buffer. The crystal oscillation frequency was recorded in EtOH (1), and changes in the frequency were monitored upon injection of **S-KAT 1** in EtOH (2), EtOH (3), water (4), pH 4.0 citrate buffer (5), **HA-GFP 6** (1 μM) in pH 4.0 citrate buffer (6), and pH 4.0 citrate buffer (7). (b) QCM trace of the control experiment using **RSR SAM** instead of **KAT-SAM**. The thickness was obtained by the simulation shown in the Supporting Information (Figure S29).

■ ASSOCIATED CONTENT

Supporting Information

The Supporting Information is available free of charge at https://pubs.acs.org/doi/10.1021/acsami.1c05652.

Syntheses of **S-KAT 1**, **HA-PEG 2** and **3**, sulfide-PEG12 **4**, sulfide-PEG120 **5**, and **HA-GFP 6** with the corresponding spectroscopic data; surface preparation and analyses by the contact angle, ellipsometry, and XPS; and QCM-D monitoring and simulation methods (PDF)

■ AUTHOR INFORMATION

Corresponding Author

Yoko Yamakoshi − *Laboratorium für Organische Chemie, ETH Zürich, CH-8093 Zürich, Switzerland;* orcid.org/0000-0001-8466-0118; Email: yamakoshi@org.chem.ethz.ch

Authors

Alessandro Fracassi − *Laboratorium für Organische Chemie, ETH Zürich, CH-8093 Zürich, Switzerland*

Ankita Ray − *Laboratorium für Organische Chemie, ETH Zürich, CH-8093 Zürich, Switzerland*

Nako Nakatsuka − *Laboratory of Biosensors and Bioelectronics, ETH Zürich, CH-8092 Zürich, Switzerland;* orcid.org/0000-0001-8248-5248

Cristiana Passiu − *Laboratory for Surface Science and Technology, Department of Materials, ETH Zürich, CH-8093 Zürich, Switzerland*
Matthias Tanriver − *Laboratorium für Organische Chemie, ETH Zürich, CH-8093 Zürich, Switzerland*
Dominik Schauenburg − *Laboratorium für Organische Chemie, ETH Zürich, CH-8093 Zürich, Switzerland*
Simon Scherrer − *Laboratorium für Organische Chemie, ETH Zürich, CH-8093 Zürich, Switzerland*
Anissa Ouald Chaib − *Laboratorium für Organische Chemie, ETH Zürich, CH-8093 Zürich, Switzerland*
Joydeb Mandal − *Laboratory for Surface Science and Technology, Department of Materials, ETH Zürich, CH-8093 Zürich, Switzerland; School of Chemistry, IISER Thiruvananthapuram, Thiruvananthapuram, Kerala 695551, India*
Shivaprakash N. Ramakrishna − *Laboratory for Surface Science and Technology, Department of Materials, ETH Zürich, CH-8093 Zürich, Switzerland*
Jeffrey W. Bode − *Laboratorium für Organische Chemie, ETH Zürich, CH-8093 Zürich, Switzerland;* orcid.org/0000-0001-8394-8910
Nicholas D. Spencer − *Laboratory for Surface Science and Technology, Department of Materials, ETH Zürich, CH-8093 Zürich, Switzerland;* orcid.org/0000-0002-7873-7905
Antonella Rossi − *Laboratory for Surface Science and Technology, Department of Materials, ETH Zürich, CH-8093 Zürich, Switzerland; Dipartimento di Scienze Chimiche e Geologiche, Università degli Studi di Cagliari, Cittadella Universitaria di Monserrato, I-09100 Cagliari, Italy*

Complete contact information is available at: https://pubs.acs.org/10.1021/acsami.1c05652

Author Contributions

A.F. and A.R. contributed equally to the manuscript. A.F., M.T., D.S., and A.O.C. synthesized the molecules under the guidance of J.W.B. and Y.Y. A.R. prepared the surface samples and performed contact angle and ellipsometry analyses under the guidance of S.N.R. and N.D.S. A.R. and C.P. performed XPS measurements and data analyses under the guidance of N.D.S. and A.R., A.F., A.R., S.S., J.M., and N.N. performed QCM measurements. N.N. and A.R. performed QCM data analyses and simulation. The manuscript was written through contributions of all authors. All authors have given approval to the final version of the manuscript.

Notes

The authors declare no competing financial interest.

■ ACKNOWLEDGMENTS

This research was supported in part by an ETH research grant (ETH-21 15-2, YY).

■ REFERENCES

(1) Wong, L. S.; Khan, F.; Micklefield, J. Selective Covalent Protein Immobilization: Strategies and Applications. *Chem. Rev.* **2009**, *109*, 4025−4053.
(2) Nakatsuka, N.; Yang, K. A.; Abendroth, J. M.; Cheung, K. M.; Xu, X. B.; Yang, H. Y.; Zhao, C. Z.; Zhu, B. W.; Rim, Y. S.; Yang, Y.; Weiss, P. S.; Stojanovic, M. N.; Andrews, A. M. Aptamer-Field-Effect Transistors Overcome Debye Length Limitations for Small-Molecule Sensing. *Science* **2018**, *362*, 319−324.
(3) Love, J. C.; Estroff, L. A.; Kriebel, J. K.; Nuzzo, R. G.; Whitesides, G. M. Self-Assembled Monolayers of Thiolates on Metals as a Form of Nanotechnology. *Chem. Rev.* **2005**, *105*, 1103−1169.
(4) Nicosia, C.; Huskens, J. Reactive Self-assembled Monolayers: from Surface Functionalization to Gradient Formation. *Mater. Horiz.* **2014**, *1*, 32−45.
(5) Cao, H. H.; Nakatsuka, N.; Deshayes, S.; Abendroth, J. M.; Yang, H. Y.; Weiss, P. S.; Kasko, A. M.; Andrews, A. M. Small-Molecule Patterning via Prefunctionalized Alkanethiols. *Chem. Mater.* **2018**, *30*, 4017−4030.
(6) Yu, Q. A.; Zhang, Y. X.; Wang, H. W.; Brash, J.; Chen, H. Anti-Fouling Bioactive Surfaces. *Acta Biomater.* **2011**, *7*, 1550−1557.
(7) Yousaf, M. N.; Mrksich, M. Diels-Alder Reaction for the Selective Immobilization of Protein to Electroactive Self-Assembled Monolayers. *J. Am. Chem. Soc.* **1999**, *121*, 4286−4287.
(8) Persson, H. H. J.; Caseri, W. R.; Suter, U. W. Versatile Method for Chemical Reactions with Self-Assembled Monolayers of Alkanethiols on Gold. *Langmuir* **2001**, *17*, 3643−3650.
(9) Abad, J. M.; Velez, M.; Santamaria, C.; Guisan, J. M.; Matheus, P. R.; Vazquez, L.; Gazaryan, I.; Gorton, L.; Gibson, T.; Fernandez, V. M. Immobilization of Peroxidase Glycoprotein on Gold Electrodes Modified with Mixed Epoxy-Boronic Acid Monolayers. *J. Am. Chem. Soc.* **2002**, *124*, 12845−12853.
(10) Devaraj, N. K.; Miller, G. P.; Ebina, W.; Kakaradov, B.; Collman, J. P.; Kool, E. T.; Chidsey, C. E. D. Chemoselective Covalent Coupling of Oligonucleotide Probes to Self-Assembled Monolayers. *J. Am. Chem. Soc.* **2005**, *127*, 8600−8601.
(11) Kuzmin, A.; Poloukhtine, A.; Wolfert, M. A.; Popik, V. V. Surface Functionalization Using Catalyst-Free Azide-Alkyne Cycloaddition. *Bioconjugate Chem.* **2010**, *21*, 2076−2085.
(12) Manova, R.; van Beek, T. A.; Zuilhof, H. Surface Functionalization by Strain-Promoted Alkyne-Azide Click Reactions. *Angew. Chem., Int. Ed.* **2011**, *50*, 5428−5430.
(13) Wagner, H.; Brinks, M. K.; Hirtz, M.; Schafer, A.; Chi, L. F.; Studer, A. Chemical Surface Modification of Self-Assembled Monolayers by Radical Nitroxide Exchange Reactions. *Chem. - Eur. J.* **2011**, *17*, 9107−9112.
(14) Kumar, R.; Ramakrishna, S. N.; Naik, V. V.; Chu, Z. L.; Drew, M. E.; Spencer, N. D.; Yamakoshi, Y. Versatile Method for AFM-Tip Functionalization with Biomolecules: Fishing a Ligand by Means of an in situ Click Reaction. *Nanoscale* **2015**, *7*, 6599−6606.
(15) Saito, F.; Noda, H.; Bode, J. W. Critical Evaluation and Rate Constants of Chemoselective Ligation Reactions for Stoichiometric Conjugations in Water. *ACS Chem. Biol.* **2015**, *10*, 1026−1033.
(16) Noda, H.; Bode, J. W. Synthesis of Chemically and Configurationally Stable Monofluoro Acylboronates: Effect of Ligand Structure on their Formation, Properties, and Reactivities. *J. Am. Chem. Soc.* **2015**, *137*, 3958−3966.
(17) White, C. J.; Bode, J. W. PEGylation and Dimerization of Expressed Proteins under Near Equimolar Conditions with Potassium 2-Pyridyl Acyltrifluoroborates. *ACS Cent. Sci.* **2018**, *4*, 197−206.
(18) Oriana, S.; Fracassi, A.; Archer, C.; Yamakoshi, Y. Covalent Surface Modification of Lipid Nanoparticles by Rapid Potassium Acyltrifluoroborate Amide Ligation. *Langmuir* **2018**, *34*, 13244−13251.
(19) Fracassi, A.; Cao, J. B.; Yoshizawa-Sugata, N.; Toth, E.; Archer, C.; Groninger, O.; Ricciotti, E.; Tang, S. Y.; Handschin, S.; Bourgeois, J. P.; Ray, A.; Liosi, K.; Oriana, S.; Stark, W.; Masai, H.; Zhou, R.; Yamakoshi, Y. LDL-Mimetic Lipid Nanoparticles Prepared by Surface KAT Ligation for in vivo MRI of Atherosclerosis. *Chem. Sci.* **2020**, *11*, 11998−12008.
(20) Pasche, S.; De Paul, S. M.; Voros, J.; Spencer, N. D.; Textor, M. Poly(L-lysine)-Graft-Poly(ethylene glycol) Assembled Monolayers on Niobium Oxide Surfaces: A Quantitative Study of the Influence of Polymer Interfacial Architecture on Resistance to Protein Adsorption by ToF-SIMS and in situ OWLS. *Langmuir* **2003**, *19*, 9216−9225.
(21) In this case, there is no functional group in PEG to react with Au surface, and ligation product **5** is expected to form similar SAM to

the one prepared from surface KAT ligation of **S-KAT** and **HA-PEG 3**.

(22) Kenausis, G. L.; Voros, J.; Elbert, D. L.; Huang, N. P.; Hofer, R.; Ruiz-Taylor, L.; Textor, M.; Hubbell, J. A.; Spencer, N. D. Poly(L-lysine)-g-Poly(ethylene glycol) Layers on Metal Oxide Surfaces: Attachment Mechanism and Effects of Polymer Architecture on Resistance to Protein Adsorption. *J. Phys. Chem. B* **2000**, *104*, 3298−3309.

(23) Dixon, M. C. Quartz Crystal Microbalance with Dissipation Monitoring: Enabling Real-Time Characterization of Biological Materials and Their Interactions. *J. Biomol. Tech.* **2008**, *19*, 151−158.

(24) Höök, F.; Rodahl, M.; Brzezinski, P.; Kasemo, B. Energy Dissipation Kinetics for Protein and Antibody-Antigen Adsorption under Shear Oscillation on a Quartz Crystal Microbalance. *Langmuir* **1998**, *14*, 729−734.

(25) Reviakine, I.; Johannsmann, D.; Richter, R. P. Hearing What You Cannot See and Visualizing What You Hear: Interpreting Quartz Crystal Microbalance Data from Solvated Interfaces. *Anal. Chem.* **2011**, *83*, 8838−8848.

(26) Sauerbrey, G. Verwendung Von Schwingquarzen Zur Wagung Dunner Schichten Und Zur Mikrowagung. *Z. Phys.* **1959**, *155*, 206−222.

(27) Vogt, B. D.; Lin, E. K.; Wu, W. L.; White, C. C. Effect of Film Thickness on the Validity of the Sauerbrey Equation for Hydrated Polyelectrolyte films. *J. Phys. Chem. B* **2004**, *108*, 12685−12690.

(28) Voinova, M. V.; Jonson, M.; Kasemo, B. 'Missing Mass' Effect in Biosensor's QCM Applications. *Biosens. Bioelectron.* **2002**, *17*, 835−841.

(29) Noda, H.; Eros, G.; Bode, J. W. Rapid Ligations with Equimolar Reactants in Water with the Potassium Acyltrifluoroborate (KAT) Amide Formation. *J. Am. Chem. Soc.* **2014**, *136*, 5611−5614.

(30) Hink, M. A.; Griep, R. A.; Borst, J. W.; van Hoek, A.; Eppink, M. H. M.; Schots, A.; Visser, A. J. W. G. Structural Dynamics of Green Fluorescent Protein Alone and Fused with a Single Chain Fv Protein. *J. Biol. Chem.* **2000**, *275*, 17556−17560.

https://doi.org/10.1021/acsami.1c05652
ACS Appl. Mater. Interfaces 2021, 13, 29113−29121